Journal of Statistical Mechanics: Theory and Experiment
An IOP and SISSA journal

Structural properties of particle deposits at heterogeneous surfaces

D Stojiljković[1], J R Šćepanović[1], S B Vrhovac[1] and N M Švrakić[1,2]

[1] Institute of Physics Belgrade, University of Belgrade, Pregrevica 118, Zemun 11080, Belgrade, Serbia

[2] Texas A&M University at Qatar, Doha, Qatar
E-mail: vrhovac@ipb.ac.rs

Received 17 March 2015
Accepted for publication 23 May 2015
Published 23 June 2015

Online at stacks.iop.org/JSTAT/2015/P06032
doi:10.1088/1742-5468/2015/06/P06032

Abstract. The random sequential adsorption (RSA) approach is used to analyze adsorption of spherical particles of a fixed radius on nonuniform flat surfaces covered by rectangular cells. The configuration of the cells (heterogeneities) was produced by performing RSA simulations to a prescribed coverage fraction $\theta_0^{(\mathrm{cell})}$. Adsorption was assumed to occur if the particle (projected) center lies within a rectangular cell area, i.e. if sphere touches the cells. The jammed-state properties of the model were studied for different values of cell size α (comparable with the adsorbing particle size) and density $\theta_0^{(\mathrm{cell})}$. Numerical simulations were carried out to investigate adsorption kinetics, jamming coverage, and structure of coverings. Structural properties of the jammed-state coverings were analyzed in terms of the radial distribution function $g(r)$ and distribution of the Delaunay 'free' volumes $P(v)$. It was demonstrated that adsorption kinetics and the jamming coverage decreased significantly, at a fixed density $\theta_0^{(\mathrm{cell})}$, when the cell size α increased. The predictions following from our calculation suggest that the porosity (pore volumes) of deposited monolayer can be controlled by the size and shape of landing cells, and by anisotropy of the cell deposition procedure.

Keywords: adsorbates and surfactants (theory), stochastic processes (theory)

1742-5468/15/P06032+23$33.00

Contents

1. Introduction

Recent developments in new and emerging technologies have generated increased demand for nano and micro-sized particles with carefully tailored properties for use in applications such as photonics, micro-electronics, plasmonics, biosensors, bio-medical devices, etc. In many applications, such nanoparticles are often integrated onto surfaces in the form of deposits in order to achieve improved performance and/or new functionalities of the final product. Thus, in addition to specific requirements for particles of definite shape, size, internal structure, surface properties or chemical composition, it is also important to be able to manipulate collective arrangements of such particles with firm control over the morphology and structure of their surface layers. To achieve this goal, the supporting surfaces are frequently prepatterned to form the templates favoring particle attachments at specific locations [1,2], or dimples, or along specified shapes, regular or otherwise [3,4]. With the use of photolithographic techniques, high-power lasers [1], chemical treatments, etc, such surface modifications are routinely realized on the microscale, but the trend is towards the nanosize patterning [1–4].

In contrast with homogeneous surfaces, the prepatterned *heterogeneous* substrates are designed with preferential attachment sites, or regions [4]. Thus, it is of theoretical and experimental interest to understand and analyze how specific surface modifications affect the morphology of deposited layers, late-stage kinetics of attachment, etc. Our analysis, described below, focuses on structural properties of particle deposits and is applicable to the presence of *randomness* in surface patterning on the scales comparable to particle size.

doi:10.1088/1742-5468/2015/06/P06032

J. Stat. Mech. (2015) P06032

Specifically, in the present work, we report a study of the irreversible deposition of spherical particles on flat nonuniform substrates covered by rectangular cells onto which the particles can adhere. The adsorption sites (landing cells) have finite size, comparable with the adsorbing particle size. We consider the process of the irreversible random sequential adsorption (RSA) of fixed size disks (projection of spherical particles). RSA is a process in which the objects of specified shape are randomly and sequentially deposited onto a substrate [5–10]. The particle-particle interaction is incorporated by rejection of deposition overlap (the hard sphere model), while the particle-substrate interaction is modeled by the irreversibility of deposition. Adsorption attempt of a particle at a randomly chosen cell is abandoned if there is an overlap with a previously adsorbed one, at the same or at a neighboring cell. Since the dominant effect in RSA is the blocking of the available surface area, after sufficiently long time a jammed state is reached when there is no more possibility for a deposition event on any landing cell. In this work we focus on the jammed-state properties.

There is a well-developed literature on irreversible adsorption on heterogeneous surfaces where particles are represented as hard spheres that bind to adsorption sites [10–15]. Our present model represents a generalized version of deposition on a random site surface (RSS), where the sites are represented by randomly distributed points [11,13]. Adamczyk *et al* [14] has extended the RSS model to the situation where the size of the landing sites, in the shape of circular disks, is finite and comparable with the size of adsorbing spheres. The available surface function, adsorption kinetics, jamming coverage, and the structure of the particle monolayer were determined as a function of the site density and the particle/site size ratio.

The motivation of our present work comes from Margues *et al* [16] and Araújo *et al* [17], who investigated the adsorption of disk-shaped particles on a patterned substrate. The pattern consisted of equal square cells centered at the vertices of a square lattice. They studied the effect of the presence of a regular substrate pattern and particle polidispersity on the deposit morphology and density, as well as on the in-cell particle population. A specific distribution function was used to describe the degree to which the cell pattern affects the overall structure of the adsorbed layer for various values of cell size and cell–cell separation parameters. It was found that the structural organization of the deposit could be latticelike, locally homogeneous, and locally oriented.

The present work is focused on the effect of the presence of randomness in substrate pattern on the structural properties of the disordered jammed state. Our aim is to quantify structural changes of the jamming covering associated with different cell size and density. Analysis at the 'microscopic' scale is based on the Voronoï tessellation [18]. Voronoï tessellation divides a two-dimensional region occupied by disks into space filling, nonoverlapping convex polygons. Further, the Delaunay triangulation is used to quantify the volume distribution of pores $P(v)$ for disk monolayers deposited on a heterogeneous substrate. This quantity has been widely used to characterize the structure of disordered granular packings and to quantify the structural changes during compaction process [19–23]. We choose as our additional tool of exploration the shape of radial correlation function $g(r)$ [24]. This is because this function provides a simple yet powerful encoding of the distribution of interparticle gaps. We also study the effect of the presence of a regular substrate pattern on the temporal evolution of the coverage fraction $\theta(t)$ and the pore distribution $P(v)$. The pattern consists of an array of cells centered on the vertices of a square lattice [16,17].

J. Stat. Mech. (2015) P06032

The following section 2 describes the details of our numerical simulations. We present simulation results and discussions in section 3. Finally, section 4 contains some additional comments and concluding remarks.

2. Model and numerical simulation

We study irreversible monolayer deposition of identical disks (sphere projections) with hard-core exclusion on a prepared flat nonuniform substrate. The substrate heterogeneities are represented by non-overlapping rectangular cells that are randomly placed and fixed on the substrate surface. The basic assumption of our model is that a particle can only be adsorbed if it is in contact with one of the cells, i.e. if the center of its disk-shaped projection lies within one of the rectangles. The substrates can be prepared in a number of ways by arranging the rectangles to form different patterns, e.g. by placing the midpoint of rectangles at the vertices of a square or triangular lattice (regular pattern), or by performing random deposition (random pattern), the procedure adopted in our work. We consider particles of fixed radius, comparable with the typical geometrical cell length. Moreover, we assume that the size of the particles is much larger than the length scale between binding sites, so that adsorption over the length scales of cell linear dimensions can be regarded as an off-lattice process. We impose the condition that deposited particles can neither diffuse along, nor desorb from the substrate on the time scales of the dense coverage formation. These assumptions are typical of the RSA model.

The simplest RSA model is defined by the following three rules: (i) objects are placed one after another at a random position on the substrate; (ii) adsorbed objects do not overlap; and (iii) adsorbed objects are permanently fixed to their spatial positions. The kinetic properties of a deposition process are described by the time evolution of the coverage $\theta(t)$, which is the fraction of the substrate area covered by the adsorbed particles. Within a monolayer deposit, each adsorbed particle affects the geometry of all later placements. Due to the blocking of the substrate area by the previously adsorbed particles, at large times the coverage approaches the jammed-state value θ_{J}, where only gaps too small to accommodate new particles (provided their centers fall within landing cells) are left in the monolayer.

The entire simulation procedure consisted of two main stages:

1. The simulation area was covered with identical rectangles (or squares) to a prescribed coverage fraction $\theta_0^{(\mathrm{cell})} < \theta_{\mathrm{J}}^{(\mathrm{cell})}$, where $\theta_{\mathrm{J}}^{(\mathrm{cell})}$ is the jamming coverage for landing cells. During this stage the usual RSA simulation algorithm was used. In this way we are able to prepare the randomly patterned heterogeneous substrate with a statistically reproducible density $\theta_0^{(\mathrm{cell})}$.

2. Then, for each initially prepared configuration, we switch the cell deposition events off and initiate a random deposition of disks, with diameter d_0, by choosing at random their position within the simulation area. The overlapping test between disks was carried out by considering the distances between the disk centers. A disk deposition attempt fails if disk's center falls outside the deposited landing cells, or if the arriving disk overlaps at least one of previously adsorbed ones.

J. Stat. Mech. (2015) P06032

The Monte-Carlo simulations are performed on a planar continuous substrate of size $L \times L = (256 d_0)^2$ with periodic boundary conditions. In calculations, the time t is gradually increased by an increment δt, given by $\delta t = \pi r_0^2 / L^2$, each time an attempt is made to deposit a disk of radius $r_0 = d_0/2$. Consequently, we define dimensionless parameter $t = N_{\mathrm{att}} \pi r_0^2 / L^2$, where N_{att} is the overall number of attempts to place disk particles. The dimensionless adsorption time t was set to zero at the beginning of the second stage. By plotting $\theta(t)$ versus the adsorption time t, defined above, one can simulate the kinetics of particle adsorption.

For purposes of our modeling, each landing cell is a rectangle with sides a and b ($b \leqslant a$) whose midpoint is located on a continuous substrate. The cells can take arbitrary orientations, but in some numerical simulations we have introduced anisotropy in the deposition procedure for landing cells. This simple modification introduces a preferential direction in the deposition process and, depending on the aspect ratio of deposited rectangles, imposes specific 'patterning' on the deposited layer. We rescale the lengths relative to the diameter of the disks d_0, and define three dimensionless parameters:

$$\alpha = \frac{a}{2r_0}, \quad \beta = \frac{b}{2r_0} \tag{1}$$

$$\gamma = \frac{\alpha}{\sqrt{\theta_0^{(\mathrm{cell})}}} \tag{2}$$

The parameter γ (an average distance between cell centers) is a meaningful measure only if the landing cells are squares ($a = b$).

For a fixed values of parameters α and β, simulations were carried out for various values of $\theta_0^{(\mathrm{cell})}$, ranging from 0.10 to 0.50. For each case, the simulations are carried out up to 10^{10} deposition attempts, or up until $L^2 \times 10^4$ consecutive deposition attempts are rejected. The results are obtained by averaging over 100 simulation runs.

3. Results and discussion

In the first part of this section simulation results are presented and discussed for random deposition of identical disks on nonuniform substrates covered by squares of arbitrary orientation. We characterize the jammed state in terms of radial distribution function of distances between the particle centers and distribution of the Delaunay 'free' volumes. After that, further analysis is extended to adsorption of disks on rectangular cells deposited with arbitrary or fixed orientation.

3.1. Circles on squares

First, we consider the irreversible deposition of disks of fixed diameter $d_0 = 1$ whose centers are inside the square cells arranged randomly at the surface. Depending on the cell size α, one can place one or more disk centers inside each cell. We are interested in the range of α where the number of disks adsorbed per cell is a small number (less than five). For $\alpha < 1/\sqrt{2}$, at most a single disk can be adsorbed at any given square cell. We denote this case as single particle per-cell adsorption (SPCA). For

squares with $\alpha \geqslant 1/\sqrt{2}$, more than a single disk can be placed in the square cell, and we denote this as multiparticle per-cell adsorption (MPCA). The cases of up-to-two, -three and -four disks per square cell are obtained, respectively, for α in the ranges $1/\sqrt{2} \leqslant \alpha < (1+\sqrt{3})/(2\sqrt{2})$, $(1+\sqrt{3})/(2\sqrt{2}) \leqslant \alpha < 1$, and $1 \leqslant \alpha < \sqrt{2}$. In other words, the numbers $\{\alpha_k : k = 1,2,3,4\} = \{1/\sqrt{2},\ (1+\sqrt{3})/(2\sqrt{2}),\ 1,\ \sqrt{2}\}$ determine the size of the largest cell in which at most $k = 1,\ 2,\ 3,\ 4$ disks can be deposited, respectively.

The effect of density of landing cells $\theta_0^{(\mathrm{cell})}$ on the adsorption process is illustrated in figure 1 by snapshots of the jammed-state coverings for (a) $\theta_0^{(\mathrm{cell})} = 0.3$ and (b) $\theta_0^{(\mathrm{cell})} = 0.5$, for two values of the cell size α, namely, $\alpha_4 = \sqrt{2} \approx 1.41$ (figure 1(a)) and $\alpha_2 = (1+\sqrt{3})/(2\sqrt{2}) \approx 0.966$ (figure 1(b)). For low values of $\theta_0^{(\mathrm{cell})}$, adsorption on a given cell is weakly affected by disks previously adsorbed on neighboring cells. Therefore, most of the cells shown in figure 1(a) contain at least three discs. However, in the case shown in figure 1(b) one can see a significant impact of the cell–cell excluded volume interaction on the cell population. Although each cell has enough area to accommodate up to two disks, only one disk is deposited on most of the cells.

3.1.1. Densification kinetics. Kinetics of the irreversible deposition of disks is illustrated in figures 2(a)–(e) where the plots of time coverage behavior $\theta(t)$ are given for the five values of coverage fraction of landing cells, $\theta_0^{(\mathrm{cell})} = 0.1,\ 0.2,\ 0.3,\ 0.4,\ 0.5$. Here the plots of such time-dependence are shown for various values of the cell size, α_k $(k = 1,2,3,4)$. It can be seen that for a fixed density of landing cells $\theta_0^{(\mathrm{cell})}$, jamming coverage $\theta_{\mathrm{J}} = \lim_{t\to\infty}\theta(t)$ decreases with increasing the cell size α_k. This effect is clearly visible in the case of the lowest density of the landing cells $\theta_0^{(\mathrm{cell})} = 0.1$ (figure 2(a)), when the average distance between the squares γ (equation (2)) is several times larger than the diameter of the disks. Then, the cell–cell separation is large enough so that adsorption on a given cell is negligibly affected by disks previously adsorbed on neighboring cells. Therefore, for sufficiently low densities $\theta_0^{(\mathrm{cell})} \lesssim 0.2$, the global kinetics of deposition is determined by the kinetics of independent adsorption processes on finite-size substrates (landing cells) with specific boundary conditions (disks can be adsorbed on finite $\alpha \times \alpha$ square as long as their centers are within the square). Consequently, for this range of $\theta_0^{(\mathrm{cell})}$ values, formula $\theta_{\mathrm{J}} = (\pi/4\alpha^2)\langle n\rangle\theta_0^{(\mathrm{cell})}$ gives very close estimation of the jamming density θ_{J}, where $\langle n\rangle$ is the mean number of disks per cell. The dashed (black) line in figure 3 shows the simulation results for the mean number of particles per cell $\langle n\rangle$ as a function of the cell size α in the noninteracting cell–cell adsorption regime (i.e. in the case of single cell on a substrate).

Consider now the case of up-to-two disks per square cell ($\alpha_2 = (1+\sqrt{3})/(2\sqrt{2}) \approx 0.966$), when $\langle n\rangle \lesssim 1.6$ (see, figure 3). Then, during the deposition process, disk can be adsorbed at the position inside the cell that blocks the chance for other disks to be adsorbed on the same cell at later times. Consequently, the probability of having a second adsorbed particle in any given cell is smaller than the probability of having at least one particle adsorbed on it. Similar reasoning applies as α crosses $\alpha_3,\ \alpha_4, \ldots$. In addition, in figure 3 we show simulation results for the probability that the configurations with only one disk, or $n = 2, \ldots, 5$ disks, occur on square cell of size α in the noninteracting cell–cell adsorption regime. If $\alpha = \alpha_1 \approx 0.707$, each landing cell (square) can contain no more than one disk. If $\alpha = \alpha_2 \approx 0.966$, the number of cells with one and two disks is

J. Stat. Mech. (2015) P06032

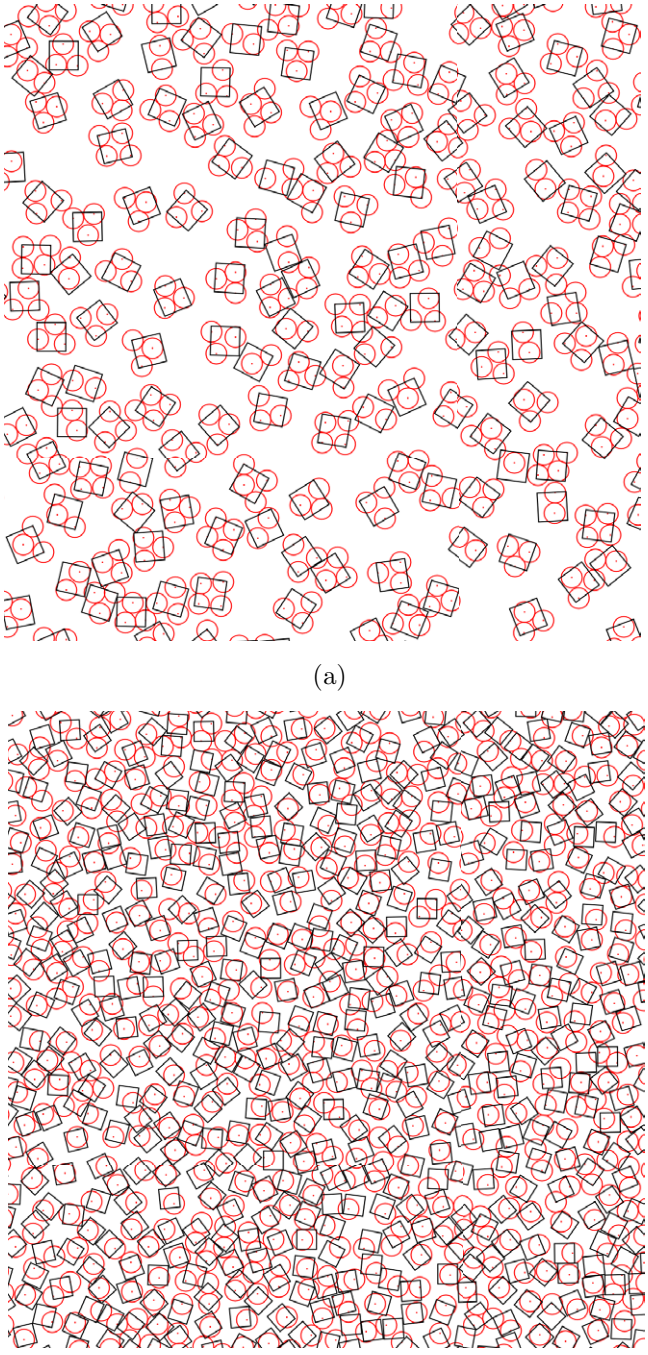

(a)

(b)

Figure 1. Typical jammed-state configuration of a region of size 30×30 in units of the disk diameter d_0, for (a) $\theta_0^{(\mathrm{cell})} = 0.3$, $\alpha_4 = \sqrt{2} \approx 1.41$, and (b) $\theta_0^{(\mathrm{cell})} = 0.5$, $\alpha_2 = (1+\sqrt{3})/(2\sqrt{2}) \approx 0.966$.

approximately equal (figure 3). However, if density $\theta_0^{(\mathrm{cell})}$ is unchanged, then the increasing of the cell size $\alpha_1 \to \alpha_2$ reduces the total number of landing cells on the substrate by a factor ≈ 2. Reduction in number of adsorbed disks is a consequence of these two effects.

doi:10.1088/1742-5468/2015/06/P06032

J. Stat. Mech. (2015) P06032

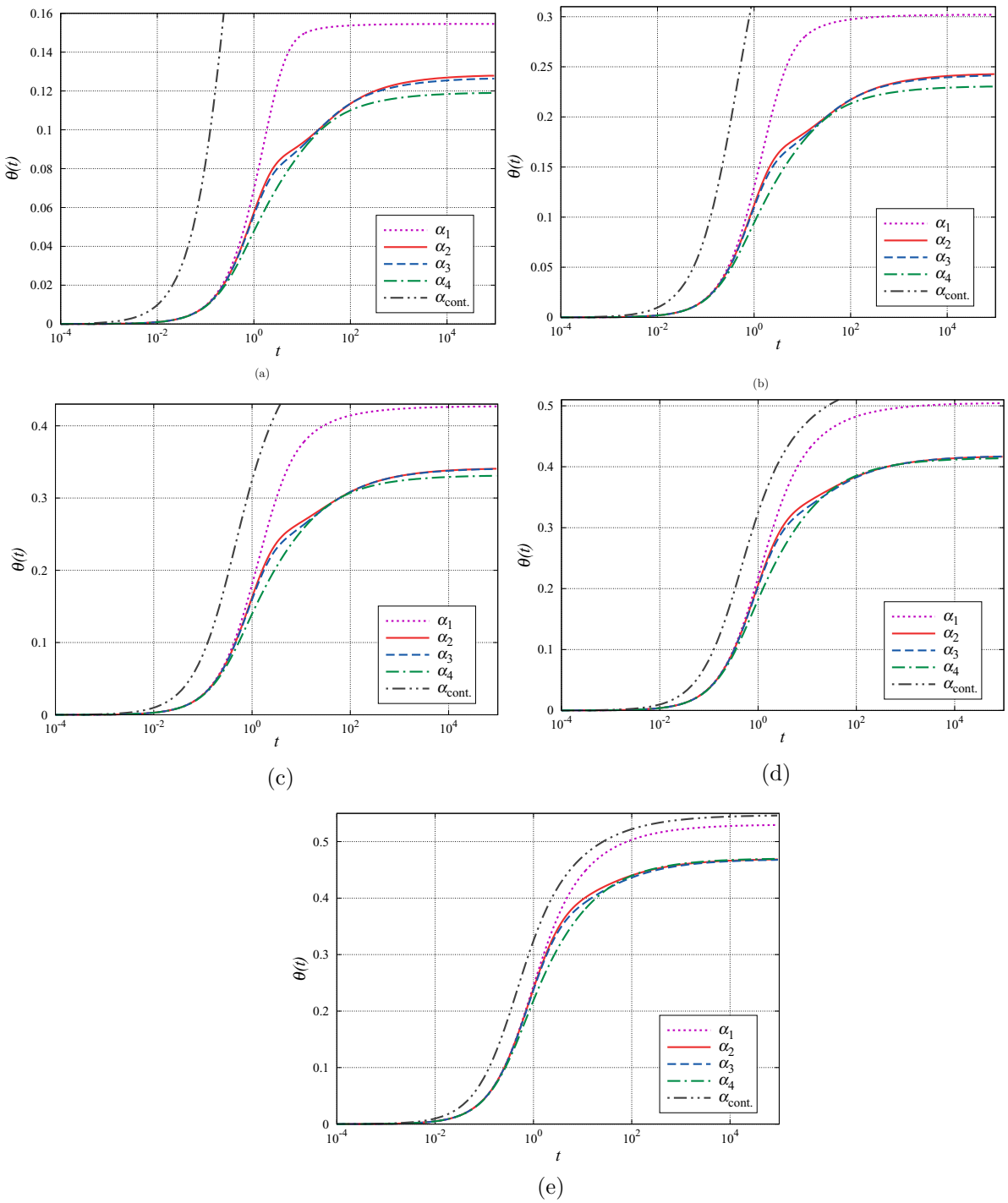

Figure 2. Shown here is the time evolution of the coverage fraction $\theta(t)$ for the five values of density of landing cells, $\theta_0^{(\mathrm{cell})} = 0.1$ (a), 0.2 (b), 0.3 (c), 0.4 (d), 0.5 (e). The curves in each graph correspond to various values of the cell size, α_k $(k = 1, 2, 3, 4)$, as indicated in the legend. The α_{cont} line shows the time dependence of the coverage $\theta(t)$ for RSA of disks on a continuous substrate. The entire α_{cont} curve can be seen in plot (e).

J. Stat. Mech. (2015) P06032

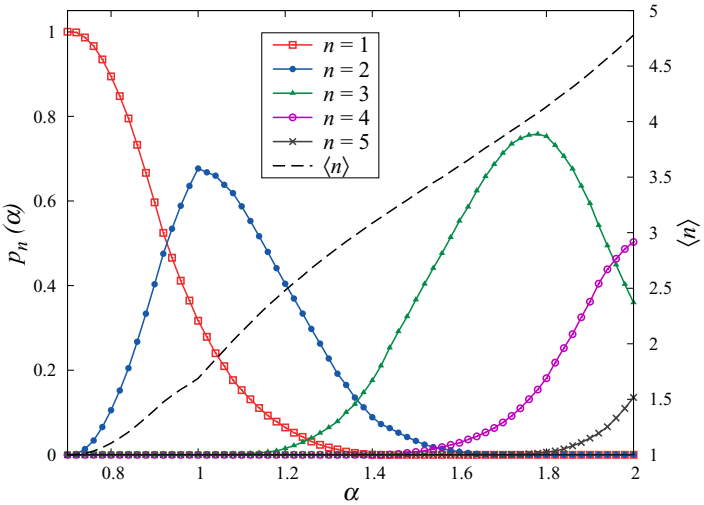

Figure 3. Simulation results for the probability that the configurations with $n = 1, 2, \ldots, 5$ disks occur on square cell of size α in the noninteracting cell–cell adsorption regime (left-hand axis). The dashed line is plotted against the right-hand axis and gives the simulation results for the average number of particles per cell $\langle n \rangle$ as a function of the cell size α in the noninteracting cell–cell adsorption regime.

This discussion indicates that the jamming density θ_J decreases with cell size α at fixed density $\theta_0^{(\mathrm{cell})}$.

As can be seen from figure 2, the time coverage behavior $\theta(t)$ is markedly slowed down with the increase of the cell size α for the fixed density of landing cells $\theta_0^{(\mathrm{cell})}$. Indeed, in MPCA case the large times are needed for filling of small isolated vacant targets on landing cells, remaining in the late stages of deposition. Furthermore, in this regime, density curves $\theta(t)$ show a noticeable slowing down of deposition process at coverages that are significantly smaller than jamming densities. Coverage growth starts to slow down at the moment when the number of adsorbed disks reaches the number of landing cells. After this initial filling of the landing cells, adsorption events take place on isolated islands of partially occupied cells. This extends the time interval between successful consecutive adsorption events and causes a slowing down of the densification.

The results for the time evolution of the coverage $\theta(t)$ in the case of up-to-two disks per square cell ($\alpha = \alpha_2$) are shown in figure 4 for various values of $\theta_0^{(\mathrm{cell})}$. Qualitatively similar results are obtained with landing cells of other sizes α. As expected, the jamming density θ_J increases with higher coverage fraction of landing cells $\theta_0^{(\mathrm{cell})}$. At high values of $\theta_0^{(\mathrm{cell})} \lesssim 0.5$ when $\gamma \sim 1$, a disk attempting adsorption can overlap with a previously adsorbed one belonging to a different cell, resulting in a failed adsorption attempt. This excluded volume interaction between particles during adsorption at *different* cells causes even slower asymptotic approach of the coverage fraction $\theta(t)$ to its jamming limit. In addition, the analysis of the time evolution of the coverage $\theta(t)$ was carried out for deposition on square cells centered at the vertices of a square lattice. Consequently, the temporal evolution of the coverage $\theta(t)$ obtained for regular substrate pattern are included in figure 4. Here, the size α and density $\theta_0^{(\mathrm{cell})}$ of landing cells are the same as those used in

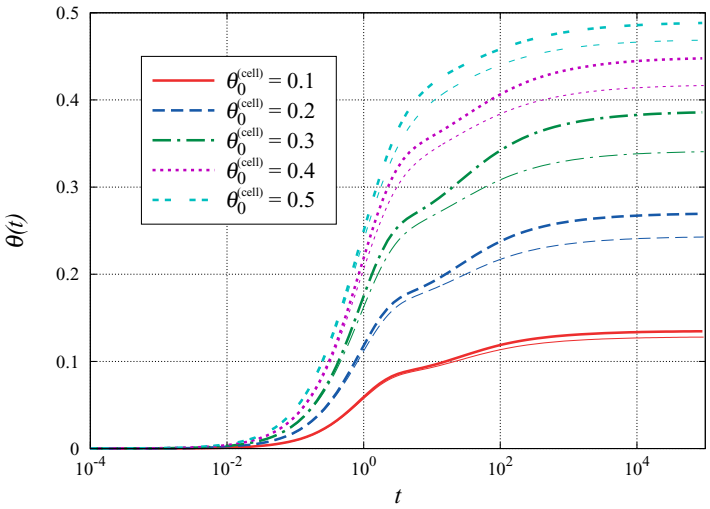

Figure 4. Temporal behavior of the coverage $\theta(t)$ for various values of $\theta_0^{(\mathrm{cell})}$ in the case of up-to-two disks per square cell (cell size: $\alpha_2 = (1+\sqrt{3})/(2\sqrt{2}) \approx 0.966$). The curves correspond to various values of density $\theta_0^{(\mathrm{cell})} = 0.1$–$0.5$, as indicated in the legend. Thick lines represent results obtained for regular substrate pattern while thin lines are results for random pattern case.

our previous calculations for random pattern case. It can be seen that lower values of the jamming coverage fraction are reached by the deposition process involving randomness in the pattern compared to a deposition process in the presence of a regular substrate pattern, regardless of the value of the density $\theta_0^{(\mathrm{cell})}$.

Below we try to characterize quantitatively the time dependence of the approach to the jammed state at large times. Depending on the system of interest modeled by RSA, the substrate can be continuous (off lattice) or discrete. Asymptotic approach of the coverage fraction $\theta(t)$ to its jamming limit, $\theta_{\mathrm{J}} = \theta(t \to \infty)$, is known to be given by an algebraic time dependence for continuous substrates [25–29]:

$$\theta(t) \sim \theta_{\mathrm{J}} - At^{-1/d}, \tag{3}$$

where A is a constant coefficient and d is interpreted as substrate dimension [26] in case of spherical particles adsorption or, more generally, as a number of degrees of freedom [30]. For lattice RSA models, the approach to the jamming coverage is exponential [31–36]:

$$\theta(t) \sim \theta_{\mathrm{J}} - \Delta\theta \ \exp(-t/\sigma), \tag{4}$$

where parameters θ_{J}, $\Delta\theta$, and σ depend on the shape and orientational freedom of depositing objects [34, 36].

Representative examples of the double logarithmic plots of the first derivative of coverage $\theta(t)$ with respect to time t are shown in Figure 5(a), for various values of the cell size, α_k $(k = 1, 2, 3, 4)$, and for high density of landing cells, $\theta_0^{(\mathrm{cell})} = 0.5$. The time derivatives of $\theta(t)$ are calculated numerically from the simulation data. In the case of the algebraic behavior of the coverage fraction $\theta(t)$ (equation (3)), a double logarithmic plot of the first time derivative $\frac{\mathrm{d}\theta}{\mathrm{dt}} \propto t^{-\frac{1+d}{d}}$ is a straight line. One can see that curves shown in figure 5(a) are straight lines in the late stage of deposition process. However, the same is not valid for all values of densities of landing cells $\theta_0^{(\mathrm{cell})}$. The double logarithmic plots

J. Stat. Mech. (2015) P06032

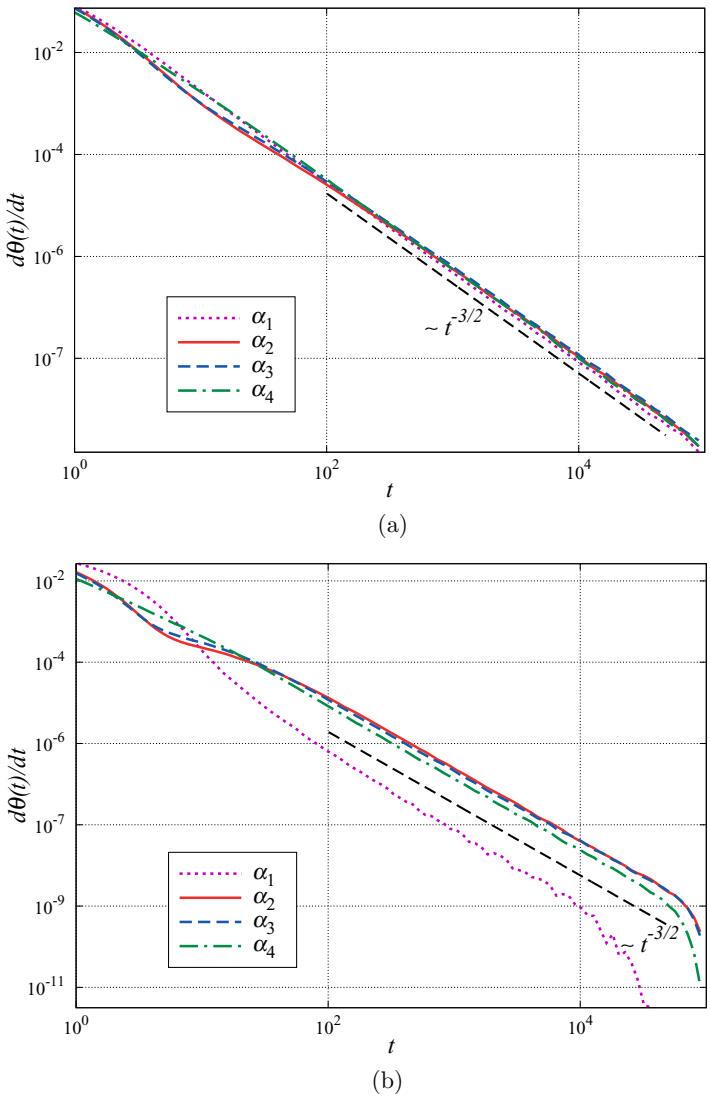

Figure 5. Test for the presence of the algebraic law (3) in the approach of the coverage $\theta(t)$ to the jamming limit for different densities of landing cells: (a) $\theta_0^{(\mathrm{cell})} = 0.5$, and (b) $\theta_0^{(\mathrm{cell})} = 0.1$. The curves in each graph correspond to various values of the cell size, α_k $(k = 1, 2, 3, 4)$, as indicated in the legend. Straight line sections of the curves show where the law holds. The dashed black line has slope $-3/2$ and is a guide for the eye.

of the numerically calculated derivatives of $\theta(t)$ for the data obtained in the case of low density of landing cell $\theta_0^{(\mathrm{cell})} = 0.1$ are shown in figure 5(b). As it can be seen, at the very late times of the deposition process the plot of the first derivative of coverage fraction $\theta(t)$ with respect to time t is not linear on a double logarithmic scale, indicating that the approach to the jamming limit is not consistent with the power law behavior given by equation (3). The deviation from the power law is particularly pronounced in the case of single particle per-cell adsorption (SPCA).

Kinetics of the irreversible deposition under SPCA conditions is illustrated in figure 6 where a logarithmic plots of $\theta_{\mathrm{J}} - \theta(t)$ versus t are shown for various densities of landing

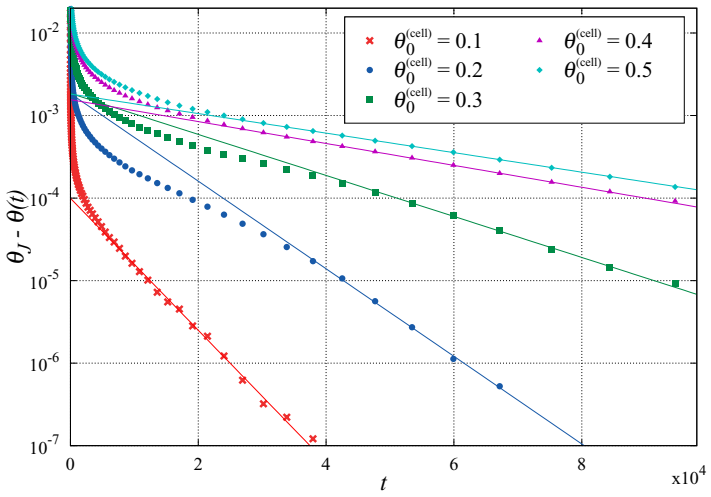

Figure 6. Plots of $\theta_J - \theta(t)$ versus t in the single particle per-cell adsorption case for various densities of landing cells $\theta_0^{(cell)} = 0.1$–0.5. The solid lines are the exponential fit of equation (4).

cells $\theta_0^{(cell)}$. These plots are straight lines for the late times of deposition, suggesting that in the case of SPCA the approach to the jamming limit is indeed exponential, as in lattice RSA models. Indeed, the kinetics of deposition in SPCA case is determined by the kinetics of adsorption processes on finite-size landing cells. The difference relative to the lattice RSA is in the particle positions, which here are uncertain within the order of the size of the cell.

3.1.2. Radial distribution function. Here we compare quantitatively the structural characteristics of jamming coverings corresponding to different values of the cell size α for various densities $\theta_0^{(cell)}$. In order to gain basic insight into the 'microstructure' of the jammed state, we first consider the radial distribution function $g(r)$ (or pair-correlation function) which gives information about the long-range interparticle correlations and their organization [24]. In absence of external forces, the pair correlation function can be calculated from expression

$$g(r) = \frac{S}{N}\frac{\overline{N}_a(r)}{2\pi r \Delta r}, \tag{5}$$

where r is the radial coordinate, S is the surface area, N is total number of particles adsorbed over this area, and $\overline{N}_a$ is the averaged number of particles within the annulus of the radius r and the thickness Δr. In figure 7(a) we compare the radial distribution function $g(r)$ at various densities $\theta_0^{(cell)} = 0.1$–0.5 in the SPCA case. As expected, the random deposition process never leads to correlation distances between the deposited particles exceeding two or three particle diameters. The position of the first peak measures typical distances between the closest disks. Decreasing the value of $\theta_0^{(cell)}$ in the SPCA case increases the uncertainty in the position of the particles which leads to peak broadening. The shape of radial distribution $g(r)$ is more structured at higher densities, showing higher first and second peaks, because, when the system gets denser, particles will be deposited closer to one another. As can be seen from figure 7(a), the minima of $g(r)$ curves shift to

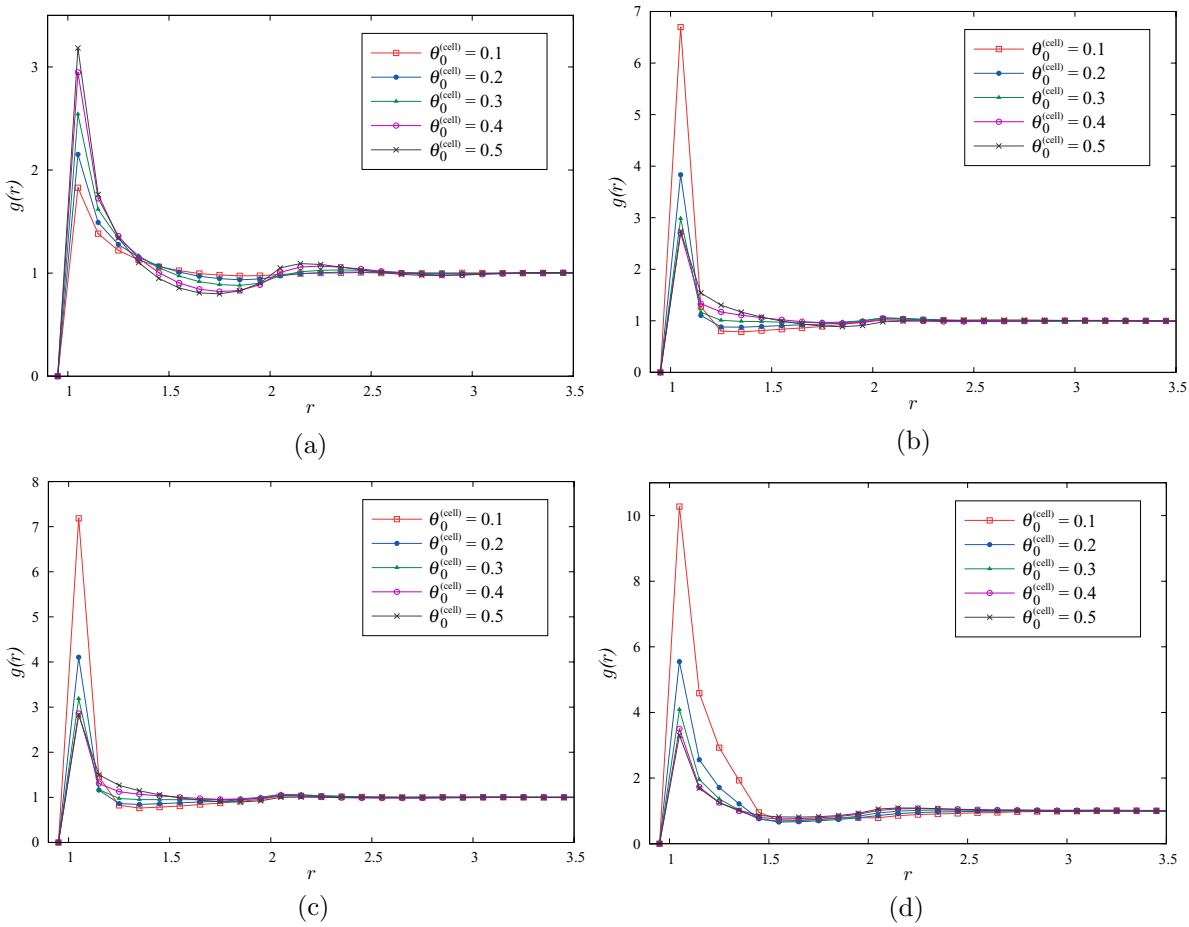

Figure 7. Radial distribution function $g(r)$ for jamming coverings as a function of separation r (in units of the disk diameter d_0) for various values of the cell size α: (a) $\alpha_1 = 1/\sqrt{2}$, (b) $\alpha_2 = (1+\sqrt{3})/(2\sqrt{2})$, (c) $\alpha_3 = 1$, (d) $\alpha_4 = \sqrt{2}$. The curves in each graph correspond to various values of density $\theta_0^{(\mathrm{cell})} = 0.1$, 0.2, 0.3, 0.4, 0.5, as indicated in the legend.

shorter distances ($\sim \sqrt{3}$) when the density $\theta_0^{(\mathrm{cell})}$ increases. At a very low densities, the broad minima are located near the distance $\sim 2d_0$. Indeed, since the particles are added at random, the probability that disks are connected as a three-bead chain is negligible.

The results for $g(r)$ in the MPCA case are shown in figures 7(b)–(d). The shape of the radial distribution function $g(r)$ is significantly affected by the values of the cell size α. In the case of up-to-two disks per square cell (figure 7(b)) the peak which appears at unit distance is the most pronounced for low densities of landing cells $\theta_0^{(\mathrm{cell})}$. For low values of $\theta_0^{(\mathrm{cell})}$, one expects a lower impact of the cell–cell excluded volume interaction on the cell population. However, as $\theta_0^{(\mathrm{cell})}$ increases, the first peak of $g(r)$ becomes broader because excluded volume interaction with disks belonging to neighboring cells reduces the average number of adsorbed disks per cell. This is opposite to what is observed under SPCA conditions (figure 7(a)), where the distance to the closest disk, on average, is determined by the distance of the nearest-neighbor landing cells.

The comparison of figures 7(b) and (c) shows that the results for $g(r)$ in the case of up-to-two and up-to-three disks per square cell are very similar. This arises as a direct consequence of the fact that cells with sizes $\alpha_2 \approx 0.966$ and $\alpha_3 = 1$ have very similar population of particles (see figure 3). Figure 7(d) shows the radial distribution function $g(r)$ of jamming coverings at several densities $\theta_0^{(\mathrm{cell})}$ obtained in simulations carried out with the cell size of $\alpha_4 = \sqrt{2}$. For this value of the parameter α, each cell is of sufficient size to accommodate up to four particles. As can be seen in figures 7(b)–(d), increasing the value of parameter α in the MPCA case increases the uncertainty in the position of the disk within the cell, i.e. it leads to peak broadening.

3.1.3. Volume distribution of the pores. Further analysis is based on the Voronoï tessellation, which allows us to unambiguously decompose any arbitrary arrangement of disks into space-filling set of cells. Given a set $\mathcal{A}$ of discrete points in the plane π (centers of disks), for almost any point $x \in \pi$ in the plane π there is one specific point $a_i \in \mathcal{A}$ which is closest to x. The set of all points of the plane which are closer to a given point $a_i \in \mathcal{A}$ than to any other point $a_j \neq a_i$, $a_j \in \mathcal{A}$, is the interior of a convex polygon $\mathcal{P}_i$ usually called the Voronoï cell of a_i. The set of the polygons $\{\mathcal{P}_i\}$, each corresponding to (and containing) one point $a_i \in \mathcal{A}$, is the Voronoï tessellation corresponding to $\mathcal{A}$, and provides a partitioning of the plane π. Voronoï cells are convex and their edges join at trivalent vertices, i.e. each vertex is equidistant to three neighboring disks. Two disks sharing a common cell edge are neighbors. In this work, the Quickhull algorithm [37] is used to compute the Voronoï diagrams in MATLAB® for a given set of disks on a plane.

The jammed-state coverings are analyzed in terms of volume distributions of the pores. The convenient definition of a pore is based on the Delaunay triangulation (DT), which is a natural way to subdivide a 2D structure of disks into a system of triangles with vertices at the centers of neighboring disks. Consequently, the circle circumscribing a Delaunay triangle has its center at the vertex of a Voronoï polygon. In this work we define the pore as a part of the Delaunay triangle not occupied by the disks (Delaunay 'free' volume) [21, 22]. The pore volume v is normalized by the 'volume' of the disks, $v_0 = d_0^2\pi/4$. In figure 8 we show Delaunay triangulation of typical jammed-state covering obtained for the same conditions as in figure 1(a) ($\theta_0^{(\mathrm{cell})} = 0.3$, $\alpha_4 = \sqrt{2} \approx 1.41$). Looking at the diagram of figure 8, one can observe variations in the area of Delaunay triangles, which indicates the presence of pores of various sizes in the deposit.

Here we consider the probability distribution $P(v)$ of the Delaunay 'free' volume v. The distribution function $P(v)$ represents the probability of finding a pore with volume v. Fluctuations in the measurements of $P(v)$ are reduced by averaging over 100 different simulations, performed under the same conditions. We compare volume distribution of the pores $P(v)$ for jamming coverings corresponding to different values of the cell size α and various densities of landing cells $\theta_0^{(\mathrm{cell})}$, as illustrated in figures 9(a)–(e). Here, the pore distributions $P(v)$ obtained for densities $\theta_0^{(\mathrm{cell})} = 0.1,\ 0.2,\ 0.3,\ 0.4,\ 0.5$ have been plotted. At very low value of $\theta_0^{(\mathrm{cell})} = 0.1$ (figure 9(a)), the curves of volume distribution $P(v)$ are asymmetric with a quite long tail on the right-hand side, which progressively reduces while the cell size α increases at the fixed density. At the same time, the distribution $P(v)$ becomes narrower and more localized around the low values of the pore volume v.

J. Stat. Mech. (2015) P06032

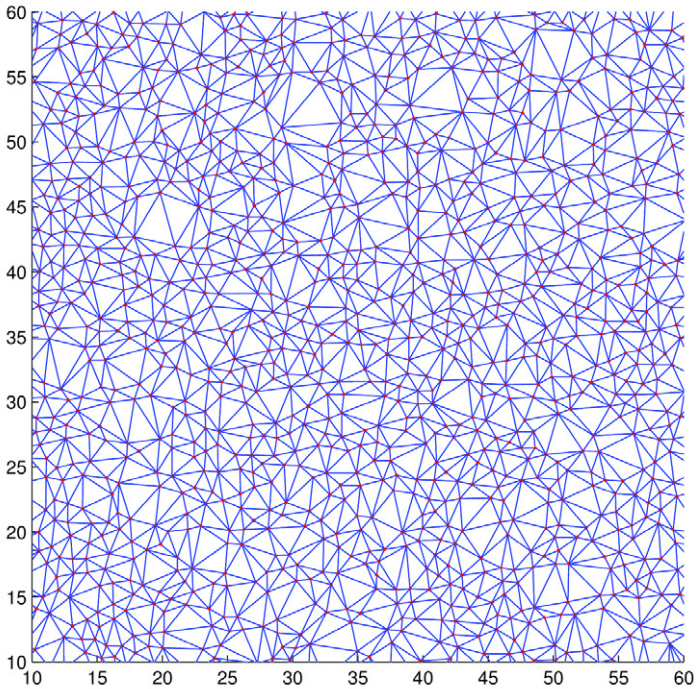

Figure 8. Delaunay triangulation of a set of points (centers of disks). Diagram corresponds to jammed-state covering obtained for density of landing cells $\theta_0^{(\mathrm{cell})} = 0.3$ and cell size $\alpha_4 = \sqrt{2}$; see figure 1(a) for a typical configuration. The red dots are centers of the adsorbed disks. Length is measured in units of the disk diameter d_0.

This behavior of the distribution $P(v)$ was not observed for all densities of landing cells $\theta_0^{(\mathrm{cell})} = 0.1$–$0.5$ (see figures 9(a)–(e)). For densities $\theta_0^{(\mathrm{cell})} \geqslant 0.2$, the pore distributions $P(v)$ obtained for deposition on square cells of size α_2 and α_3 are broader and shifted to higher values of volumes v compared to the pore distribution $P(v)$ corresponding to SPCA case (α_1). Qualitative interpretation of this result is given below.

In the case of up-to-four disks per square cell ($\alpha_4 = \sqrt{2}$), we observe the appearance of pronounced peak of $P(v)$ at low values of v, approximately at $v = 0.15$–0.20. It is easy to understand which kind of local configuration contributes mostly to this peak of the $P(v)$. The Delaunay cells with free dimensionless volume $v_{\mathrm{hex}} = \sqrt{3}/\pi - 1/2 \approx 0.051$ correspond to the local arrangements of hexagonal symmetry, when three disks are all in touch with each other with centers on the vertices of a unilateral triangle. The cells with free volume $v_{\mathrm{quad}} = 2/\pi - 1/2 \approx 0.13$ correspond to the local configurations of quadratic symmetry, when centers of four touching disks are positioned on the vertices of a square. These are minimal values of pore volumes that can be formed with three and four disks deposited on a single landing cell of size $\alpha_4 = \sqrt{2}$. However, the probability that the previously described structures of quadratic and hexagonal symmetry arise during the process of random deposition is negligibly small. Therefore, the 'free' volumes formed with random deposition of disks into a single cell are larger than the minimal values $v_{\mathrm{hex}} \approx 0.051$ and $v_{\mathrm{quad}} \approx 0.13$, so that observed peak of $P(v)$ is around $v \lesssim 0.20$.

J. Stat. Mech. (2015) P06032

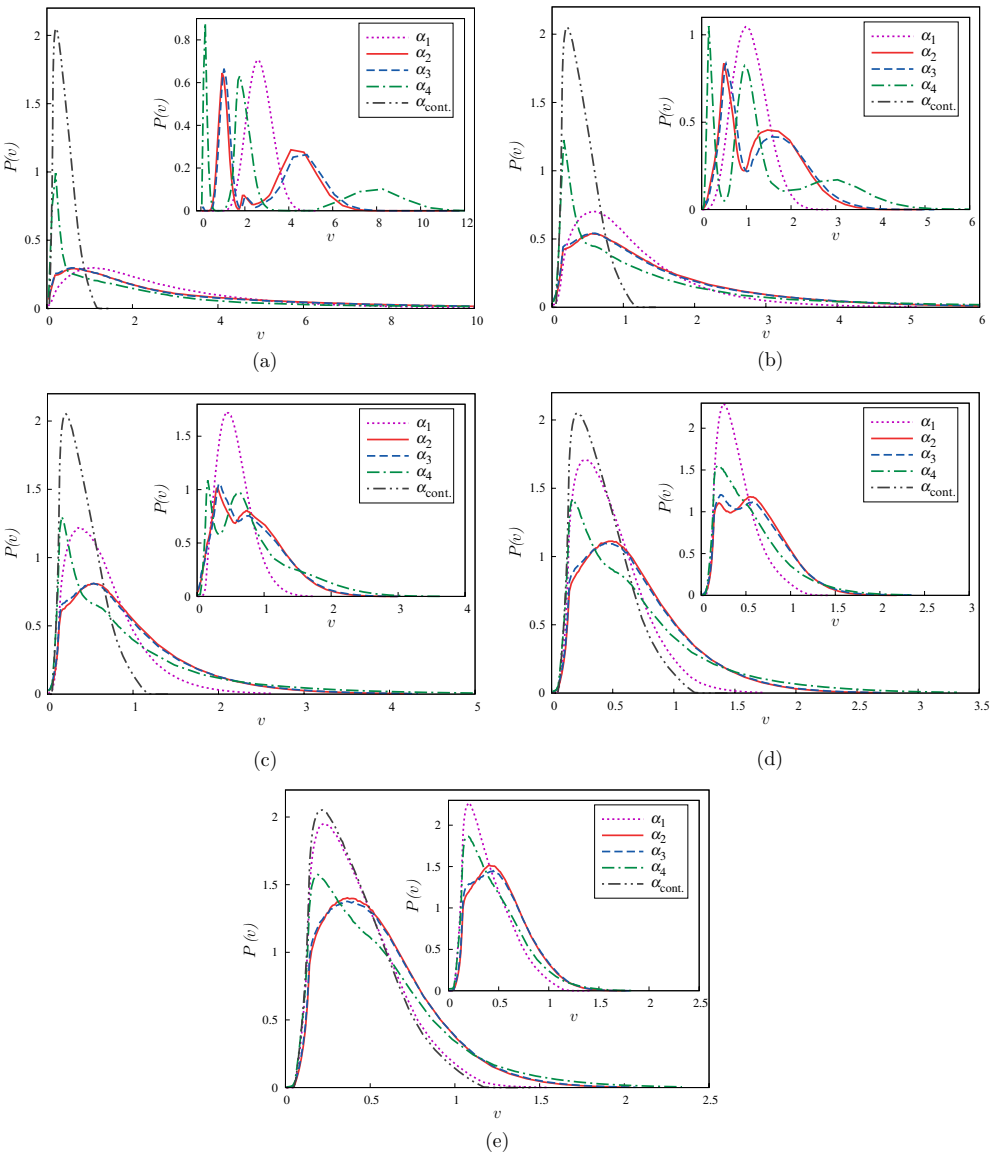

Figure 9. Main panel: Volume distribution of the pores $P(v)$ for jamming coverings at different values of density of the landing cells corresponding to $\theta_0^{(\mathrm{cell})} = 0.1$ (a), 0.2 (b), 0.3 (c), 0.4 (d), 0.5 (e) are shown in the case of random pattern. The curves in each graph correspond to various values of the cell size, α_k $(k = 1, 2, 3, 4)$, as indicated in the legend. The α_{cont} line shows distribution $P(v)$ for jamming covering in the case of the irreversible disks deposition on a continuous substrate. Insets: Volume distribution of the pores $P(v)$ for jamming coverings obtained from simulations carried out using the heterogeneous surface covered by square cells centered at the vertices of a square lattice. The size α and density $\theta_0^{(\mathrm{cell})}$ of landing cells are the same as those used in the main panel.

At high values of density of landing cells $\theta_0^{(\mathrm{cell})} = 0.5$ (figure 9(e)), distribution $P(v)$ obtained under SPCA conditions becomes very similar to pore volume distribution for RSA of disks on a continuous substrate, as expected. The results for the volume distribution of the pores $P(v)$ obtained in the cases of up-to-two and up-to-three disks

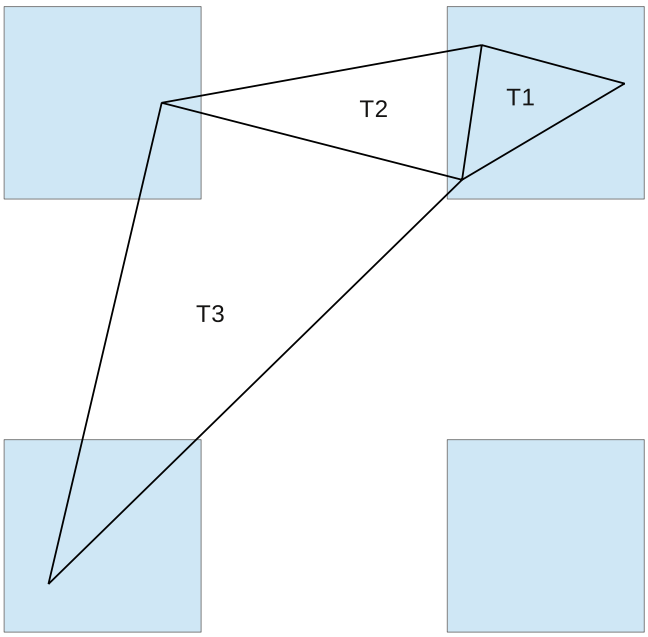

Figure 10. Various types of Delaunau triangles (T1–T3) depending on the position of vertices.

per square cell are almost identical at all densities $\theta_0^{(\mathrm{cell})}$ (see figure 9). The similarity of these distributions at small values of pore volumes can be explained by the results shown in figure 3. Small pores appear due to the presence of configurations with three or more disks on a single landing cell. But, in the case of up-to-three disks per square cell, the number of in-cell configurations with three disk is considerably smaller than the number of configurations with one or two disks. Consequently, broad maximum in $P(v)$, centered at $v = 0.4$–0.6 is caused by contribution of large pores formed mostly in the space between the landing cells.

Further, we study the effect of the presence of a regular substrate pattern of squares on volume distribution of the pores $P(v)$. Distributions $P(v)$ for jamming coverings corresponding to $\theta_0^{(\mathrm{cell})} = 0.1$–$0.5$ and different values of the cell size α_k $(k = 1, 2, 3, 4)$ are shown in insets of figure 9. At low density of landing cells $\theta_0^{(\mathrm{cell})} = 0.1$ and for large cell size $\alpha \geqslant \alpha_4 = \sqrt{2}$ (see inset of figure 9(a)) we observe the appearance of three peaks of $P(v)$. The first peak at $v \approx 0.2$ is due to Delaunay triangles with their vertices inside a single landing cell (see T1 triangle in figure 10). The third peak at $v \approx 8$ corresponds to Delaunay triangles with vertices located in different landing cells (see T3 triangle in figure 10). Central peak at $v \approx 2$ arises due to Delaunay triangles with two vertices belonging to single cell, while the third one is located in a neighboring cell (see T2 triangle in figure 10). The first peak at very low values of pore volumes v does not appear for the smaller landing cells, $\alpha = \alpha_1,\ \alpha_2,\ \alpha_3$. Indeed, if $\alpha \leqslant \alpha_3$, the Delaunau triangles that lie within a single landing cell are very rare $(\alpha = \alpha_3)$ or they can not exist $(\alpha \leqslant \alpha_2)$. In the case of single particle per-cell adsorption $(\alpha = \alpha_1)$ vertices of each Delaunay triangle are located in three different cells, so that distribution $P(v)$ has only one broad maximum. As can be seen from insets of figure 9, the difference between distribution $P(v)$ for regular

J. Stat. Mech. (2015) P06032

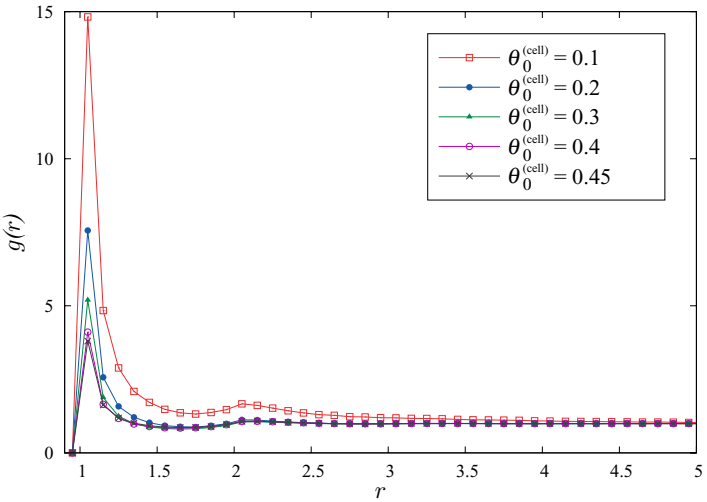

Figure 11. Radial distribution function $g(r)$ for jamming coverings as a function of separation r (in units of the disk diameter d_0) obtained from simulations carried out using the heterogeneous surface covered by rectangles of arbitrary orientation. The curves correspond to various values of density $\theta_0^{(\mathrm{cell})} = 0.1$, 0.2, 0.3, 0.4, 0.45, as indicated in the legend.

substrate pattern of squares and for random pattern case decreases with the increase of the cell density $\theta_0^{(\mathrm{cell})}$.

3.2. Circles on rectangles

We have also performed numerical simulations of random deposition of identical disks on heterogeneous surfaces covered by rectangles of arbitrary orientation. In these simulations, each landing cell is a rectangle with sides $\alpha = 8$ and $\beta = 1$ (in units of the disk diameter d_0). The choice of the value of aspect ratio α/β plays important role in our model. Increasing of the aspect ratio of the landing cells (rectangles) leads to the formation of domains of increased regularity. The chosen value of $\alpha/\beta = 8$ is large enough to provide patterned substrate that is significantly different from the surfaces in the case with the square cells. We have verified that usage of a different, but large, values of aspect ratio α/β gives quantitatively very similar results leading to qualitatively same phenomenology.

To characterize the jammed state we studied radial distribution function $g(r)$ and probability distribution $P(v)$ of pore volume v for different values of density of landing cells: $\theta_0^{(\mathrm{cell})} = 0.1,\ 0.2,\ 0.3,\ 0.4,\ 0.45$. Figure 11 shows the corresponding results for radial distribution function $g(r)$. Comparing the results from figures 7(b)–(d) and 11, one can see that the first peak near $r/d_0 = 1$ and local maximum at $r/d_0 \gtrsim 2$ of $g(r)$ are more pronounced in the case of elongated rectangular cells than in the case of multi-particle adsorption (MPCA) at squares. This emergence of a better local order is a correlation effect that develops during the deposition stage, due to the formation of arrays of disks along a single elongated rectangular cells.

Figure 12 compares volume distribution of the pores $P(v)$ for jamming coverings corresponding to different densities $\theta_0^{(\mathrm{cell})}$. Similar to the case of MPCA on square cells,

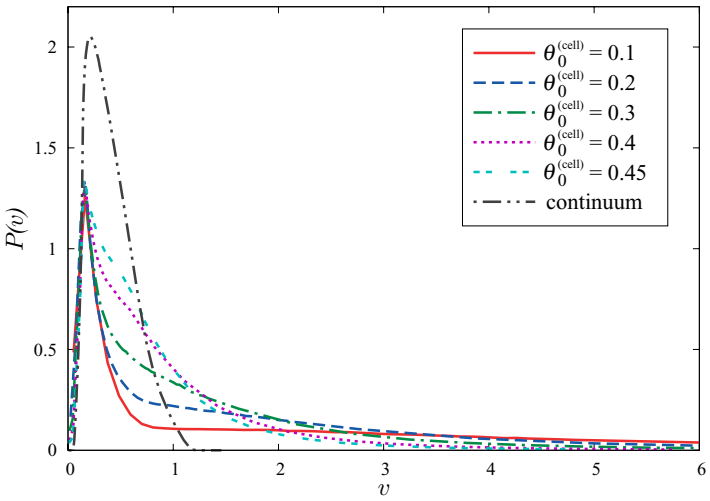

Figure 12. Volume distribution of the pores $P(v)$ obtained from simulations carried out using the heterogeneous surface covered by rectangles of arbitrary orientation. The curves correspond to various values of density $\theta_0^{(\mathrm{cell})} = 0.1$, 0.2, 0.3, 0.4, 0.45, as indicated in the legend. Distribution $P(v)$ for jamming covering in the case of the irreversible disks deposition on a continuous substrate is shown for comparison.

here we observe the peak of $P(v)$ at small values of $v \approx 0.2$. As previously mentioned, such small pores are feature of coverings which occurs when three or more particles can be adsorbed on a single cell. The observed peak of the distribution $P(v)$ broadens when density $\theta_0^{(\mathrm{cell})}$ increases. Deposition of elongated objects at high densities is characterized with compact domains of parallel objects and large islands of unoccupied substrate area. Figure 13 shows typical snapshot of the jammed-state covering obtained for rectangular cells of arbitrary orientation and density $\theta_0^{(\mathrm{cell})} = 0.45$. Relatively high local packing of nearly parallel adsorbed rectangles reduces the number of disks effectively adsorbed at a cell. This process is associated with the appearance of larger interstitial voids, which causes the peak broadening.

It is now useful to explore the interplay between the anisotropy in deposition procedure for landing cells and structural characteristics of jamming coverings. In this case the orientation of rectangular cells is fixed to the one preferential direction. The configuration formed in the long time regime is made up of a large number of domains; see figure 14 for typical configuration. As expected, any such domain contains parallel cells all close to each other. This produces better packing of landing cells and higher impact of the cell–cell excluded volume interaction on the average cell population. Hence, anisotropic deposition of landing cells lowers the average cell population, which enhances the appearance of larger pores, resulting in a peak broadening. Volume distributions of pores $P(v)$ for jamming coverings of disks corresponding to anisotropic deposition of cells are shown in figure 15 with thick lines, while the case of arbitrarily oriented cells from figure 12 is drawn with thin lines for comparison. Figure 15 clearly shows enhanced peak broadening of $P(v)$ in the case of anisotropic deposition of landing cells, which is consistent with previous discussion.

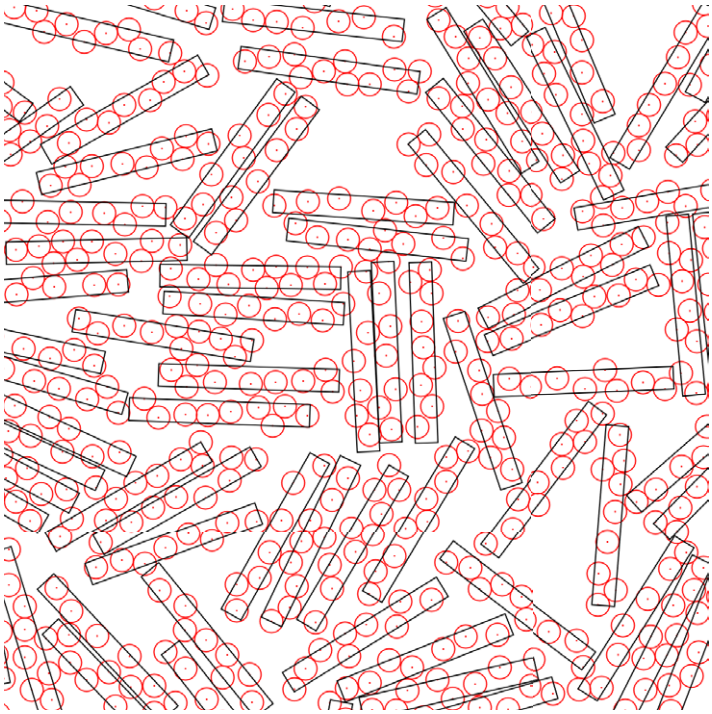

Figure 13. Typical jammed-state configuration of a region of size 30×30 (in units of the disk diameter d_0), for $\theta_0^{(\mathrm{cell})} = 0.45$. Orientation of rectangular cells with sides $\alpha = 8$ and $\beta = 1$ is arbitrary. Deposition of elongated objects (cells) is characterized with domains of nearly parallel objects and large islands of unoccupied space.

4. Concluding remarks

We investigated numerically RSA of disk-shaped particles on a nonuniform substrates, with focus on the jammed-state properties. A surface heterogeneities consisting of square cells and elongated rectangles were considered. The influence of the cell size and density of landing cells on kinetics of deposition process, and on morphological characteristics of the coverings were studied.

We found that for a given density of landing cells, the highest jamming coverage and the fastest kinetics of the deposition process can be achieved in the SPCA case. Due to the fact that the densification kinetics is dictated by geometric exclusion effects, the coverage kinetics is severely slowed down in the MPCA case.

To examine the short scale structure in the jammed-state coverings, we evaluated the radial correlation function $g(r)$ which measures the particle density-density correlation at distance r for various shapes and sizes of the landing cells. The oscillation of $g(r)$ quickly decays for all densities of landing cells $\theta_0^{(\mathrm{cell})}$, which means that long-range order does not exist in the system. In the MPCA case, the peak of $g(r)$ which appears at unit distance is the most pronounced for low densities of landing cells $\theta_0^{(\mathrm{cell})}$. This is opposite to what is observed under SPCA conditions when the shape of radial distribution $g(r)$ is more structured at higher densities $\theta_0^{(\mathrm{cell})}$.

doi:10.1088/1742-5468/2015/06/P06032

J. Stat. Mech. (2015) P06032

Figure 14. Typical jammed-state configuration of a region of size 30×30 (in units of the disk diameter d_0,) for $\theta_0^{(\mathrm{cell})} = 0.45$. Orientation of rectangular cells with sides $\alpha = 8$ and $\beta = 1$ is fixed to the horizontal direction.

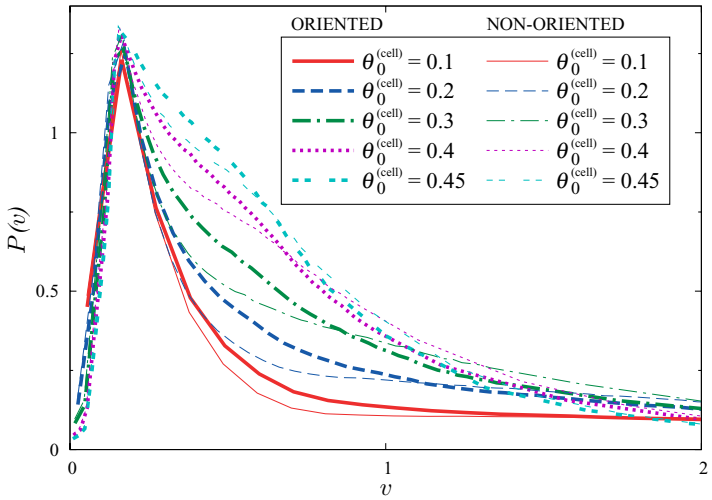

Figure 15. Volume distribution of the pores $P(v)$ obtained from simulations carried out using the heterogeneous surface covered by rectangles of fixed orientation (thick lines) and arbitrary orientations (thin lines). The curves correspond to various values of density $\theta_0^{(\mathrm{cell})} = 0.1, 0.2, 0.3, 0.4, 0.45$, as indicated in the legend.

Morphology of deposited disks has also been analyzed through the distribution of pore volumes. This distribution is sensitive to small structural changes of the covering and therefore describes the degree to which the cell size and cell density affects the deposit

morphology. Delaunay 'free' volumes have a distribution with a long tail, particularly at low densities $\theta_0^{(\mathrm{cell})}$. We have found that the distribution $P(v)$ becomes narrower and more localized around the low values of v with increasing of $\theta_0^{(\mathrm{cell})}$. In the case of the largest cells ($\alpha \geqslant \alpha_4 = \sqrt{2}$), we have observed the pronounced peak of $P(v)$ at low values of $v = 0.15$–0.20, which appears due to presence of configurations with three or more disks on a single landing cell. We have also studied the influence of a regular substrate pattern on volume distribution of the pores $P(v)$. At low densities $\theta_0^{(\mathrm{cell})}$, distribution function $P(v)$ shows a well developed peaks which correspond to the various types of Delaunay triangles, as shown in figure 10. Cell–cell excluded volume interaction increases with the cell density $\theta_0^{(\mathrm{cell})}$, so that distribution $P(v)$ for regular substrate pattern of squares becomes similar to $P(v)$ for random pattern case at densities near jamming limit for RSA of square cells.

Numerical simulations of random deposition on heterogeneous substrates covered by elongated rectangles have shown that the shape of the pore distribution function $P(v)$ is affected by the anisotropy in deposition procedure for landing cells. It is shown that anisotropic deposition of landing cells lowers the average cell population and reduces the number of small pores. Our results suggest that the porosity of deposit (pore volumes) can be controlled by the size and shape of landing cells, and by anisotropy of cell deposition procedure. It must be emphasized that radial correlation function $g(r)$ for jamming coverings of disks corresponding to anisotropic deposition of rectangles is quite similar to $g(r)$ for the case of isotropic landing-cell pattern and is not detailed here.

Acknowledgments

This work was supported by the Ministry of Education, Science and Technological Development of the Republic of Serbia, under Grant No. ON171017. Work at TAMUQ was supported by NPRP grant #6-021-1-005 and from the Qatar National Research Fund (a member of Qatar Foundation).

References

[1] Parisse P, Luciani D, D'Angelo A, Santucci S, Zuppella P, Tucceri P, Reale A and Ottaviano L 2009 Patterning at the nanoscale: atomic force microscopy and extreme ultraviolet interference lithography *Mater. Sci. Eng.* B **165** 227–30

[2] Kraus T, Malaquin L, Schmid H, Riess W, Spencer N D and Wolf H 2007 Nanoparticle printing with single-particle resolution *Nat. Nanotechnol.* **2** 570–6

[3] Kershner R J *et al* 2009 Placement and orientation of individual dna shapes on lithographically patterned surfaces *Nat. Nanotechnol.* **4** 557–61

[4] delCampo A, Greiner C, Àlvarez I and Arzt E 2007 Patterned surfaces with pillars with controlled 3d tip geometry mimicking bioattachment devices *Adv. Mater.* **19** 1973–7

[5] Flory P J 1939 Intramolecular reaction between neighboring substituents of vinyl polymers *J. Am. Chem. Soc.* **61** 1518

[6] Evans J W 1993 Random and cooperative sequential adsorption *Rev. Mod. Phys.* **65** 1281–329

[7] Privman V 2000 Dynamics of nonequilibrium deposition *Colloids Surf.* A **165** 231–40

[8] Talbot J, Tarjus G, Van Tassel P R and Viot P 2000 From car parking to protein adsorption: an overview of sequential adsorption processes *Colloids Surf.* A **165** 287–324

[9] Senger B, Voegel J C and Schaaf P 2000 Irreversible adsorption of colloidal particles on solid substrates *Colloids Surf.* A **165** 255–85
[10] Cadilhe A, Araújo N A M and Privman V 2007 Random sequential adsorption: from continuum to lattice and pre-patterned substrates *J. Phys.: Condens. Matter* **19** 065124
[11] Jin X, Wang N H L, Tarjus G and Talbot J 1993 Irreversible adsorption on non-uniform surfaces: the random site model *J. Chem. Phys.* **97** 4256
[12] Jin X, Talbot J and Wang N H L 1994 Analysis of steric hindrance effects on adsorption kinetics and equilibria *AIChE J.* **40** 1685
[13] Oleyar C and Talbot J 2007 Reversible adsorption on random site surface *Physica* A **376** 27–37
[14] Adamczyk Z, Weronski P and Musial E 2002 Irreversible adsorption of hard spheres at random site (heterogeneous) surfaces *J. Chem. Phys.* **116** 4665
[15] Adamczyk Z, Siwek B, Weronski P and Musial E 2002 Irreversible adsorption of colloid particles at heterogeneous surfaces *Appl. Surf. Sci.* **196** 250
[16] Marques J F, Lima A B, Araújo N A M and Cadilhe A 2012 Effect of particle polydispersity on the irreversible adsorption of fine particles on patterned substrates *Phys. Rev.* E **85** 061122
[17] Araújo N A M, Cadilhe A and Privman V 2008 Morphology of fine-particle monolayers deposited on nanopatterned substrates *Phys. Rev.* E **77** 031603
[18] Aurenhammer F 1991 Voronoi diagrams: a survey of a fundamental geometric data structure *ACM Comput. Surv.* **23** 345
[19] Philippe P and Bideau D 2001 Numerical model for granular compaction under vertical tapping *Phys. Rev.* E **63** 051304
[20] Richard P, Philippe P, Barbe F, Bourles S, Thibault X and Bideau D 2003 Analysis by x-ray microtomography of a granular packing undergoing compaction *Phys. Rev.* E **68** 020301
[21] Aste T 2005 Variations around disordered close packing *J. Phys.: Condens. Matter* **17** S2361–90
[22] Aste T 2006 Volume fluctuations and geometrical constraints in granular packs *Phys. Rev. Lett.* **96** 018002
[23] Arsenović D, Vrhovac S B, Jakšić Z M, Budinski-Petković Lj and Belić A 2006 Simulation study of granular compaction dynamics under vertical tapping *Phys. Rev.* E **74** 061302
[24] Truskett T M, Torquato S, Sastry S, Debenedetti P G and Stillinger F H 1998 Structural precursor to freezing in the hard-disk and hard-sphere systems *Phys. Rev.* E **58** 3083–8
[25] Feder J 1980 Random sequential adsorption *J. Theor. Biol.* **87** 237
[26] Swendsen R 1981 Dynamics of random sequential adsorption *Phys. Rev.* A **24** 504
[27] Pomeau Y 1980 Some asymptotic estimates in the random parking problem *J. Phys. A: Math. Gen.* **13** L193
[28] Bonnier B 2001 Random sequential adsorption of binary mixtures on a line *Phys. Rev.* E **64** 066111
[29] Burridge D J and Mao Y 2004 Recursive approach to random sequential adsorption *Phys. Rev.* E **69** 037102
[30] Hinrichsen E L, Feder J and Jøssang T 1986 Geometry of random sequential adsorption *J. Stat. Phys.* **44** 793–827
[31] Bartelt M C and Privman V 1990 Kinetics of irreversible multilayer adsorption: one-dimensional models *J. Chem. Phys.* **93** 6820
[32] Nielaba P, Privman V and Wang J S 1990 *J. Phys. A: Math. Gen.* **23** L1187
[33] Manna S S and Švrakić N M 1991 Random sequential adsorption: line segments on the square lattice *J. Phys. A: Math. Gen.* **24** L671–6
[34] Budinski-Petković Lj and Kozmidis-Luburić U 1997 Random sequential adsorption on a triangular lattice *Phys. Rev.* E **56** 6904
[35] Budinski-Petković Lj and Kozmidis-Luburić U 1997 Jamming configurations for irreversible deposition on a square lattice *Physica* A **236** 211–9
[36] Budinski-Petković Lj, Vrhovac S B and Lončarević I 2008 Random sequential adsorption of polydisperse mixtures on discrete substrates *Phys. Rev.* E **78** 061603
[37] Barber C B, Dobkin D P and Huhdanpaa H 1996 The quickhull algorithm for convex hulls *ACM Trans. Math. Softw.* **22** 469

J. Stat. Mech. (2015) P06032